Volume:38 No:1 2025

e-ISSN-2791-7185

TURKISH JOURNAL OF NUCLEAR SCIENCES

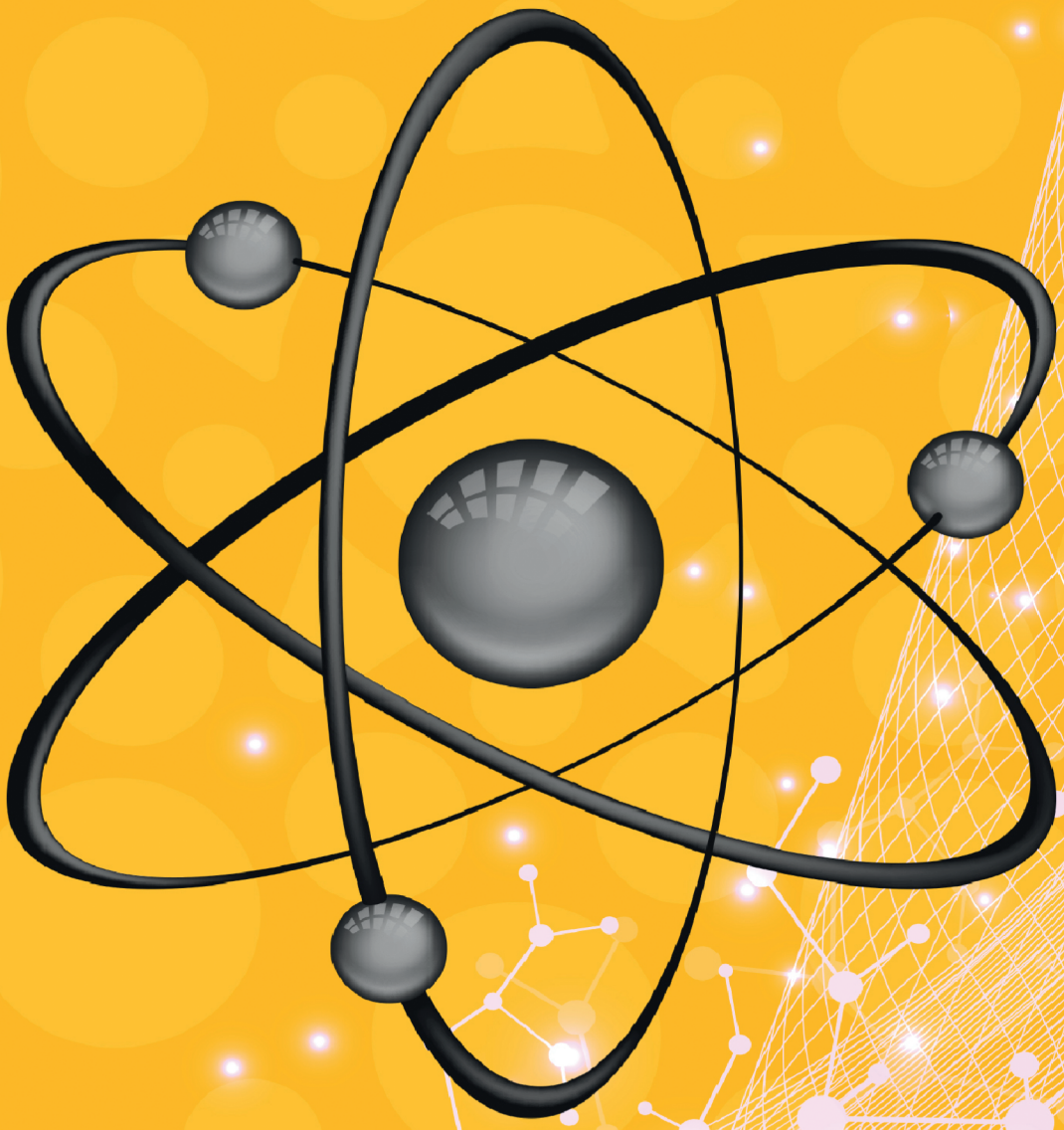

e-ISSN: 2791-7185

TURKISH JOURNAL OF NUCLEAR SCIENCES

VOL **38** ISSUE **01** YEAR **2025**

Owner on Behalf of Turkish Energy, Nuclear and Mining Research Authority (TENMAK)
President
Dr. Abdullah Buğrahan Karaveli (Ankara, Türkiye)

Editor in Chief
Doç. Dr. Semra Tepe Çam (Ankara, Türkiye)

Editor
Dr. Serdar Bulut (Ankara, Türkiye)

Publisher
TENMAK Akademi ve Yayınlar Koordinatörlüğü

Adress of Publication Manager
Ankara Üniversitesi Beşevler Kampüsü Emniyet Mahallesi
Yenimahalle, 06560, Ankara, Türkiye
Phone: (0312) 212 62 30
E-mail: journal@tenmak.gov.tr
Web: https://dergipark.org.tr/tr/pub/tjns

Type of Publication: Yaygın süreli yayın
Range of Publication: 6 Aylık
Publication Date: 30/06/2025

Turkish Journal of Nuclear Sciences is National and International refereed journal. Journal has been published twice a year, in June and December, only electronically .Please visit the Journal website https:// https://dergipark.org.tr/tjns for writing rules, copyright form and published articles.

ANKARA
JUNE 2025

TURKISH ENERGY, NUCLEAR AND MINERAL RESEARCH AGENCY
TURKISH JOURNAL OF NUCLEAR SCIENCES
E-ISSN: 2791-7185
https://dergipark.org.tr/tr/pub/tjns

İÇİNDEKİLER/CONTENTS

TURKISH ENERGY, NUCLEAR AND MINERAL RESEARCH AGENCY
TURKISH JOURNAL OF NUCLEAR SCIENCES
E-ISSN: 2791-7185
https://dergipark.org.tr/tr/pub/tjns

Pulse mode analysis of TRIGA Burned Core using thermal hydraulics code PARET/ANL

M. H. Altaf [1,*], N. H. Badrun [1]

[1] Reactor Physics and Engineering Division Bangladesh Atomic Energy Commission Ganakbari, Savar, Dhaka-1349, Bangladesh

ARTICLE INFO

Article History:
Received October 1, 2025
Available online June 30, 2025

Research Article

Keywords:
TRIGA
Burned Core
PARET/ANL
Transient Analysis

ABSTRACT

A transient-state thermal hydraulics analysis of the TRIGA burned core of the TRIGA Mark II research reactor was conducted using PARET/ANL. This study focused on calculating safety parameters due to large reactivity insertions at low operating power. The peak power and energy for the burned core were computed, whose values were found to be lower than those of the beginning of the cycle (BOC) core. Moreover, the safety parameters of DNBR and clad temperature remained well within the margins of the Safety Analysis Report (SAR). No nucleate boiling was observed in the hottest fuel. These findings indicate that the burned core can be safely utilized for pulse mode operation.

1. Introduction

TRIGA Mark II research reactor in Bangladesh was commissioned in Bangladesh in 1986. The reactor is designed for multi-purpose use, such as training, education, radioisotope production and various R&D activities including neutron activation analysis, neutron scattering, and neutron radiography [1]. Having a water-cooled and graphite-reflected core, the reactor has the capacity to operate continuously at 3 MW (thermal). The unique feature of the reactor is its substantial prompt negative temperature coefficient that can control the reactor before its engineering control system is active. The TRIGA reactor comprises 100 fuels, including 5 fuel follower control rods and 2 instrumental fuel elements. The fuel is arranged in a hexagonal array in the reactor core shroud that distributes fuel efficiently and utilizes space optimally. TRIGA reactors offer operational flexibility by functioning in both steady and transient states, notably featuring a unique pulse mode, and while they rely on natural convection for cooling up to 500 kW, forced convection is employed for operation at higher power levels.

Thermal hydraulics research primarily focuses on efficiently removing heat from the fuel under various operating, burnup, and core arrangement conditions to prevent excessive fuel temperatures, steam void formation, and approaching the hydrodynamic critical heat flux.

The unique and extreme operating feature of TRIGA reactors is pulse mode that generates immense flux for research and training when a large amount of reactivity is achieved for a short period. Even at low energy operation, usually around 100 watts, accidental initiation of large reactivity, such as from control rod blockage, can induce pulsing. While the negative temperature coefficient of the reactor inherently controls the power, rapid generation of significant power in pulse mode operation can still impose substantial thermal and mechanical stress on the fuel and core.

After 38 years of operational life, the TRIGA reactor is no longer capable of operating in full power; It is now run at low power (100 watts) to support research only. However, even at this reduced power, there is a risk of large pulsing if sufficient reactivity is suddenly introduced. Furthermore, the extensive burnup of fuel elements from fission reactions has altered the axial and radial fuel composition as the core has already experienced 800 MWDs (Mega Watt Days) of operation life. This change directly impacts the power peaking factor and heat transfer coefficients. As the core continues to experience burnup, thermal hydraulics parameters like fuel temperature and DNBR (Departure from Nucleate Boiling Ratio) - defined as the ratio of the critical heat flux to the heat flux achieved in the core - could exceed safety limits. Therefore, it is essential to study these safety parameters specifically for pulse mode operation under current burnup conditions.

Historically, several codes have been used so far to calculate the thermal-hydraulic characteristics of the Beginning of Cycle (BOC) core of the TRIGA Mark

*Corresponding author: altaf335@yahoo.com

II research reactor [2, 3]. Altaf et al. [4] conducted a thermal hydraulics study of the burned core using EUREKA-2/RR. However, EUREKA does not include Bernath correlation, which is suggested by General Atomic [5] to conduct the DNBR calculation, a crucial safety parameter. Moreover, no thermal hydraulics transient study of burned core of Bangladesh Atomic Energy Commission (BAEC) TRIGA has been performed using the PARET/ANL code, which encompasses a wide array of correlations, particularly the Bernath correlation. Therefore, safety parameters due to the insertion of a large amount of reactivity was studied in this simulation to ensure the reactor operates within the safety margin.

2. Calculation Method

The PARET/ANL [6] code possess the capability to simulate heat transfer phenomena from the fuel element to the coolant when the reactor is operating. Therefore, the PARET/ANL code was employed to calculate the transient state parameters of thermal hydraulics of the reactor. Figure 1 illustrates the configuration of the existing core of the reactor. The PARET/ANL code was chosen due to general applicability, its simplicity of coding, and rapid execution. It is designed for use in predicting the course and consequences of non-destructive reactivity accidents in small reactor cores.

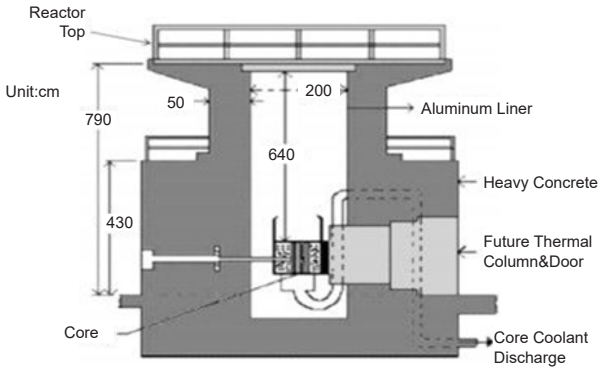

Figure 1. Cutaway view of TRIGA reactor

It is a coupled neutronic-hydrodynamic heat transfer code employing point kinetics, one-dimensional hydrodynamics, and one-dimensional heat transfer. The kinetics equations of the point reactor ensure the dynamic behavior of power within the reactor through computational analysis. The time-dependent temperatures within the fuel element are computed using a one-dimensional heat conduction equation solved in axial sections. The resolution of these equations is accomplished by estimating the reactivity feedback from the initial moment until the specific point of interest. The feedback resulting from the expansion of fuel rods, the density effects of the moderator, and the fuel temperature effect collectively contribute to the overall reactivity feedback. The PARET/ANL model consists of a water-cooled core represented by a maximum of 15 fuel elements and associated coolant channels. In our modeling, the whole core was divided into two channels, keeping the hottest rod and associated coolant in one channel and other fuel rods and coolant in the rest. All channels were divided into 10 equal nodes. Table 1 represents thermal-hydraulic operating parameters of the TRIGA.

Table 1. TRIGA fuel specifications.

Parameters	Design Value
Fuel Element (rod type)	20% w/o U-ZrH, 19.7% enriched
Total Number of fuels in the core	100
Cladding	Stainless Steel 304L
Reflector	Graphite
Inlet Temperature˚C (Full Power)	40.6
Radius of Zr rod (cm)	0.3175
Fuel radius (cm)	1.82245
Clad outer radius (cm)	1.87706
Gap width (cm)	0.00381
Active fuel length (cm)	38.1
Flow area (cm^2)	5.3326
Hydraulic Diameter (cm)	1.80594
Pressure (Pa)	1.60654×10^5
Friction Loss Coefficient	0.07
Pressure Loss Coefficient	1.81(Inlet), 2.12 (Outlet)
Pitch (cm)	4.5716
Mass flow rate, kg/m^2s	3.2089×10^3
Coolant Velocity (cm/sec)	287.58

The power peaking factors of fuel rods and axial peak-to-average ratio of the hottest rod of the 700 MWD burned core, used in this thermal hydraulics calculation, were determined using the Monte Carlo code MVP [7]. The calculation yielded the hottest rod factor of 1.668. Only peaking factor has been revised for simulating 700 MWD as no thermal properties have been reexamined here. Physical parameters and operating conditions for transient state operation for 700MWD has been kept as same as the BOC core as the core arrangement is still the same. The thermal-hydraulic calculations were carried out with a water inlet temperature of 40.6˚C and an inlet pressure of 160.6 kPa, corresponding to the static pressure of water across the reactor channels. As per the final safety analysis report (FSAR), the rate of mass flow for coolant circulation in the downward direction stands at 13248 liters per minute as per FSAR [8]. For the current study, the thermal hydraulics safety parametric study due to reactivity insertion of 1.996$ and 2.24$ at operating power of 100 watts for 0.1 sec with 0.015 delay time has been selected so that the results can be compared with already available data for the same condition of the BOC core conducted by Huda M Q [9]. Bernath correlation has been selected for DNBR calculation in this study.

3. Results and Discussions

3.1 Reactivity Insertion of 1.996$

Transients of reactor power, energy, minimum DNBR at the hottest spot of the hottest fuel, and clad temperature at the surface of the hottest fuel for reactivity insertion of 1.996$ was studied in this simulation utilizing PARET/ANL. As depicted in Figure 2, reactor power began to rise upon reactivity insertion. Although

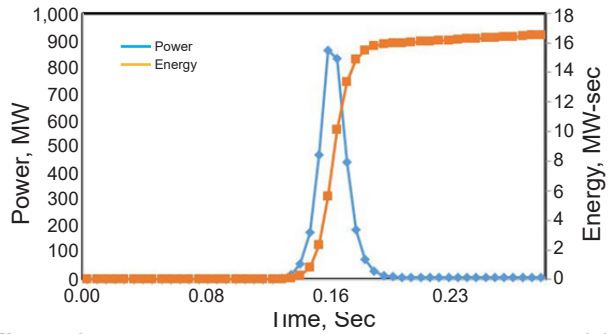

Figure 2. Power and Energy transient at 1.966$ reactivity insertion

expected to continue until the 0.1 second insertion time elapsed, a 0.015 second delay resulted in a peak power of 859.44 MW at 0.115 seconds. Subsequently, negative feedback reactivity caused power to return to its initial level by 0.18 seconds. The peak power for the same reactivity was calculated to be 873 MW in the BOC core by Huda M. Q. [9]. The power pulse's full-width half maxima was 15.8 milliseconds, further indicating the burned core is safer for pulse mode operation compared to the BOC core. Concurrently, core energy increased over time, initially rising slowly with power before accelerating significantly after 0.1 seconds, mirroring the power curve. It reached 16.5 MW-sec at 0.20 seconds before stabilizing.

DNBR stands out as a crucial parameter in the safety analysis. To prevent the most adverse combination of mechanical and coolant conditions within the core, it is imperative to maximize the value of DNBR from unity as outlined in the Safety Analysis Report. DNBR calculation over 0.40 seconds starting from arbitrary zero seconds for the reactivity insertion of 1.996$ is shown in Figure 3. The minimum DNBR over the transient time was found to be 1.59 over the simulation time, which is bigger than the SAR accepted minimum value of unity, ensuring the safety of the core at this operating condition.

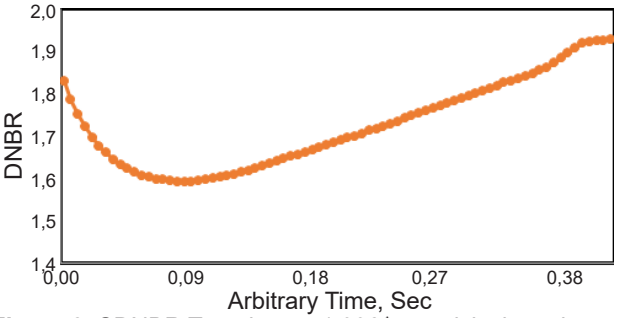

Figure 3. SDNBR Transient at 1.996$ reactivity insertion

In another study, the cladding temperature of the hottest rod for the same reactivity insertion and operating power was computed. Figure 4 shows the cladding temperature over 5 seconds from the insertion of reactivity of 1.996$. It is evident from the figure that the cladding temperature increases sharply after the insertion and reaches 133.64 °C peak temperature, compared to 144.54 °C for ERUEKA-2/RR for 2$ [10]. After that, the temperature decreases gradually until dropping down to 82.89°C at 5 seconds. No nucleate boiling has been found in the output file for the hottest fuel rod.

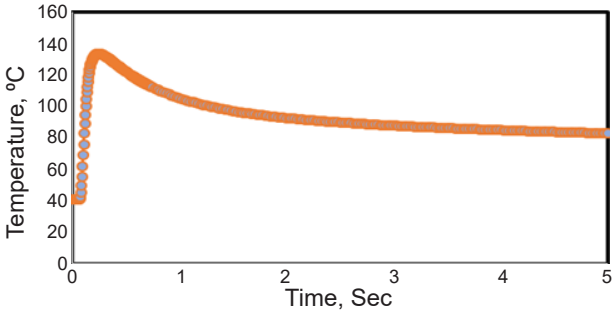

Figure 4. Temperature transient with 1.996$ reactivity insertion

3.2 Reactivity Insertion of 2.24 $

Transients of reactor power, energy, minimum DNBR at the hottest spot of the hottest fuel, and cladding temperature at the surface of the hottest fuel for the reactivity insertion of 2.24$ was studied in another simulation. As depicted in Figure 5, reactor power began to rise upon reactivity insertion. Although

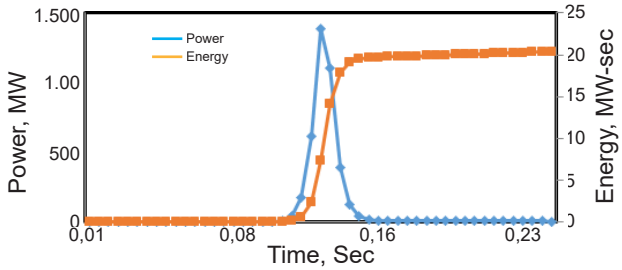

Figure 5. Power and Energy transient at 2.24$ reactivity insertion

expected to continue until the 0.1-second insertion time elapsed, a 0.015-second delay resulted in a peak power of 1385 MW at 0.15 sec. Subsequently, negative feedback reactivity caused power to return to its initial level in 0.19 seconds. The peak power for the same reactivity was calculated to be 1629 MW in the BOC core by Huda M. Q. [9]. Hence, the burned core found to be safer for pulse mode operation compared to the BOC core. The full-width half maxima of the power pulse was found to be 16.2 milliseconds, compared to 15.8 milliseconds for 1.996$.

Meanwhile, the energy of the core increased steadily over time. It began rising with the increase of power from the beginning of reactivity insertion, and then surged after 0.1 seconds, reaching 20.4 MW-sec at 0.22 seconds before stabilizing. It is worth noting that both the power and energy for the 2.24$ reactivity insertion were greater than those for the 1.996$ insertion.

DNBR calculation over 0.42 seconds after arbitrary zero seconds for reactivity insertion of 2.24$ is shown

in Figure 6. The minimum DNBR over the transient time was found to be 1.21 over the simulation time, which is less than 1.59 for a reactivity insertion of 1.996$. However, this value is bigger than the SAR accepted minimum value of unity, meaning the core operates safely for a reactivity insertion of 2.24$ during 100 watts operating power.

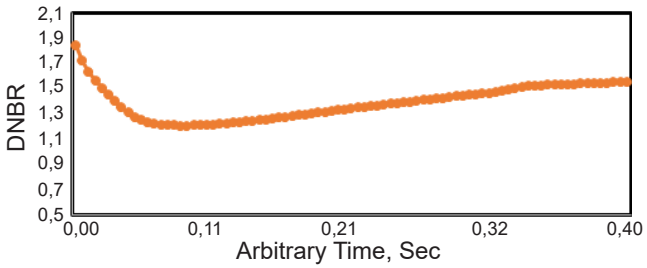

Figure 6. DNBR Transient at 2.24$ reactivity insertion

Lastly, the clad temperature for this reactivity insertion and operating power was conducted. Figure 7 shows the cladding temperature over 5 seconds from the insertion of reactivity of 2.24$. One can observe from the figure that the cladding temperature increases sharply after the insertion and reaches 139.56°C peak temperature, compared to 133.71°C for 1.996$. After that, the temperature decreases gradually till it drops down to 84°C at 5 seconds, compared to 82.89°C for 1.996$. No nucleate boiling has been observed in fuel.

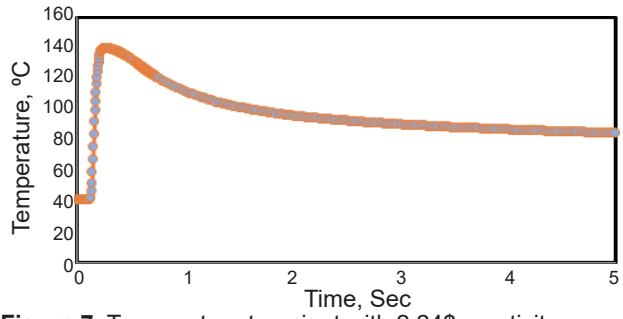

Figure 7. Temperature transient with 2.24$ reactivity insertion

4. Conclusion

The reactivity-initiated transient analysis of the 3 MW TRIGA Mark-II research reactor at Savar, Dhaka, Bangladesh, has been evaluated using PARET/ANL. The study compares the thermal hydraulics parameters of the reactor's burned core with those of its Beginning of Cycle (BOC) core. The results indicate that safety parameters for the burned core were consistently lower and no nucleate boiling was observed in any region of the hottest fuel. These findings suggest that the burned core of the 3 MW TRIGA Mark-II research reactor is safer to operate than the BOC core. Furthermore, among the two reactivity insertions in the burned core, the reactor was found to be safer for low reactivity insertion. Based on these observations, the burn-TRIGA core can be recommended for pulse mode operation.

5. Acknowledgment

The authors would like to acknowledge Argonne National Laboratory for providing the license, code, and technical support for the PARET/ANL code, and they are also thankful to the members of the Reactor Physics and Engineering Division (RPED) for their cooperation.

6. References

[1] Hossain S M, Zulquarnain M A, Kamal, I and Islam M N (2011). Current Status and Perspectives of Nuclear Reactor Based Research in Bangladesh, IAEA, Vienna, 7-14. IAEA-TECDOC-1659

[2] Mizanur Rahman M M, Akond, M A R, Basher M K, and Huda M Q (2014). Steady State Thermal Hydraulic Analysis of TRIGA Research Reactor, World Journal of Nuclear Science and Technology, 81-87

[3] Huda M Q and Rahman M (2004). Thermo-Hydrodynamic Design and Safety Parameter Studies of the TRIGA MARK II Research Reactor, Annals of Nuclear Energy, 31, 1101-1118

[4] Altaf M H and Badrun N H (2014).Thermal Hydraulic Analysis of 3 MW TRIGA Research Reactor of Bangladesh Considering Different Cycles of Burnup, Atom Indonesia, 40(3), 107-112.

[5] General Atomics (1979), 10 MW TRIGA-LEU Fuel and Reactor Design Description. General Atomics, San Diego.

[6] Obenchain, C F, PARET (1969)-A Program for the Analysis of Reactor Transients. IDO-17282, Idaho Atomic Energy.

[7] Mahmood M S et al. (2012), Individual Fuel Element Burnup of BAEC TRIGA Core, Technical Report, INST-RPED-RARD-01/009.

[8] FSAR (2006), Final Safety Analysis Report for 3 MW TRIGA MARK-II Research Reactor at AERE, Savar, Dhaka, Bangladesh. BAEC, Dhaka.

[9] Huda, M Q, Bhuiyan, S I, Chakroborty, T K, Sarker, M M and Mondal, M A W (2001). Thermal Hydraulic Analysis of the 3 MW TRIGA MARK-II Research Reactor under steady state and transient state conditions. Nuclear Technology, 135, 51-66

[10] Altaf M H, Badrun N H and Khan M J H (2014). Validation of EUREKA-2/RR Code for Analysis of Pulsing Parameters of TRIGA Mark II Research Reactor in Bangladesh, The nucleus, 53(3), 385-389

TURKISH ENERGY, NUCLEAR AND MINERAL RESEARCH AGENCY
TURKISH JOURNAL OF NUCLEAR SCIENCES
E-ISSN: 2791-7185
https://dergipark.org.tr/tr/pub/tjns

Reliability computation of kinetic energy based Shannon Entropy for tritium plasma graphene interactions

Alper Pahsa [1,*]

[1] **Havelsan Inc, Air C4ISR Systems, Ankara, 06510, Türkiye**

ARTICLE INFO

Article History:
Received April 20, 2025
Available online June 30, 2025

Research Article

Keywords:
Material Reliability of Graphene with Kinetic Energy PMI of Tritium on Graphene
Tokamak reactor graphene material reliability
Tritium based fusion reactor material reliability
Fusion reactor kinetic energy based reliability

ABSTRACT

When selecting reactor building elements, it is important to consider the structural reliability of Tokamak fusion reactors. Fusion reactions generate substantial heat and energy, which can alter the structure of reactor walls, thereby diminishing the efficiency of energy production in reactors. The primary materials employed for walls in fusion reactors include tungsten, beryllium, and graphene, owing to their high melting points. This study looks at how tritium plasma ions, which have energies between 5 and 35 keV, affect graphene wall surfaces using molecular dynamics simulations, and also assesses the system's Kinetic Energy using Shannon entropy modeling. We use this information to compute the Weibull distribution's reliability prediction for graphene structures.

1. Introduction

The Population growth and rising living standards are increasing energy demand, a serious issue in this century. Most of the energy is originated from depleting fossils. Sustainability is the main feature that is required by the nuclear and renewable energy [1-2]. Energy is created at the final stage of exothermic nuclear processes; fission and fusion are crucial nuclear processes. An unstable, big nucleus is splitted into two or more smaller particles that releases energy at the output. Fission processes are the main source of power in todays current most nuclear reactors of today. Nuclear fusion process is made up of fusing the several nuclei. It produces nuclear and subatomic particles. Energy is created as the mass changes in reactants and products in the process. Nuclear fusion process requires 100 million degrees in its process. That is why the nuclear fusion is preferred in the researches of today and future studies in which has an unlimited fuel worldwide. Safe fusion reactors for instance, produces transient radioactive waste [3-6] in their processes. The most famous fusion reaction is the process that uses tritium and deuterium. The 14 MeV neutron from this event warms water to make turbine steam. Additionally, this reaction yields 3.5 MeV He [7-9]. The produced Helium of the fusion product reactor is the input nuclei of the Deuterium and Tritium under a huge amount of heated plasma [10-11]. Classic thermonuclear fusion reactors use magnetic fields to densify the plasma. Magnetic fields trap plasma from the reactor's first wall. High-energy plasma influences barriers. The divertor zone has the highest attrition because magnetic field lines convey lower-energy plasma to the wall. Plasma-first wall materials and interactions are studied in fusion. Plasma must yield fusion helium. Helium interacts with divertor walls during removal [12-13]. Dying divertor and reactor walls discharge neutrons. Tungsten, beryllium, molybdenum, steel, and graphene inhibit tokamak reactor wall erosion. High melting point and atomic number make tungsten plasma-resistant [11-13]. Nuclear fusion reactor structural reliability analysis is unusual in reliability literature. General studies are performed for nuclear fission reactors as in structural reliability analysis. For instance [14] examines nuclear fission power plant structural system and component structural analysis with probabilistic analysis methods in determining the longevity, dependability, and danger. This source uses probability, material science, fluid, fracture, and structural mechanics. Most nuclear fusion reactors' main issue is fusion reactions. Literature understates structure reliability. In [15], recent structural and thermomechanical research are discussed including the magnet, diagnostic, and reproductive coverage. Safe and dependable systems affect fusion device dependability for creating the trust. Wendelstein 7-X, DEMO, and ITER fusion equipment for energy generation or experiments are assessed for availability, maintainability, and inspectability [13]. This study includes solely fusion device basics. Commercial plasma applications with surface coating are best for

*Corresponding author: apahsa@havelsan.com.tr

Tokamak fusion reactor structure reliability testing. Space-based plasma-facing structures must resist radiation and particles. Plasma-facing structures must resist radiation and particles to limit space impacts [15-19]. Tokamak nuclear fusion reactor walls struggled to maintain tritium. Plasma-facing graphene magnetic fusion loses tritium. Plasma tritium retention was 40% and 51% for JET and TFTR. After experiments, fusion reactor sanitization took 12–16%. Walls of titanium. To Recent calculations predict that the French experimental Tokamak reactor ITER will approach its tritium limit after 100 pulses. Rising tritium levels stretch reactor walls, shortening life. This affects thermal-to-electric energy transfer in fusion. This study used molecular dynamics simulations to develop a graphene wall structure with bigger crystal atomic patterns. In thermonuclear reactors like ITER and DEMO, where harsh conditions (high temperatures, intense neutron radiation) make traditional detectors difficult to use, graphene is being investigated as a potential material for magnetic field sensors and structural elements. Research shows that graphene-based Hall effect sensors, especially those made on silicon carbide (SiC) substrates, are remarkably resistant to radiation and retain their high sensitivity even when exposed to rapid doses of neutrons. The MARIA reactor's research verified that although neutron irradiation changes the density of charge carriers, the majority of damage is inflicted on the hydrogen passivation layer instead of the graphene, indicating the possibility of self-healing at elevated temperatures. Apart from sensors, graphene-reinforced metal nanocomposites (such those with Cu, Ni, or V) show enhanced radiation endurance by trapping flaws at interfaces, making them promising choices for reactor walls and structural materials. Moreover, graphene and carbon nanotubes are recommended for first-wall applications due to their low neutron absorption, thermal stability, and possibility for integrated cooling through capillary fluid transfer. However, molecular dynamics study emphasizes the need for perfect fabrication by showing how composite performance might be hampered by pre-existing graphene damage. Graphene's unique properties make it a crucial component for the development of fusion technology, despite persistent challenges with substrate optimization and hydrogen layer replacement.

Graphene coatings may have a number of benefits over more conventional materials like tungsten or carbon composites, according to recent research on the retention of tritium in graphene-based tokamak wall designs. According to research, few-layer graphene's poor hydrogen isotope solubility and rapid diffusion rates, which promote tritium desorption, can lower tritium retention by up to 70% when compared to graphite (e.g., Zhang et al., 2024 in Nuclear Fusion). Furthermore, the damage caused by plasma exposure is lessened by graphene's better heat conductivity and radiation resistance. However, issues remain with adhesion stability at high heat fluxes and potential defect-induced trapping at grain boundaries (Lee et al., 2023, Applied Surface Science). While graphene-covered test tiles on EAST and DIII-D show promising reductions in co-deposition, the effects of prolonged exposure to neutrons are still being investigated. Graphene's scalability may enable self-cleaning walls with smaller tritium reserves, but more research is required before big divertors can employ it.

The following figure 1 shows the initial configuration of the study model system in the simulation:

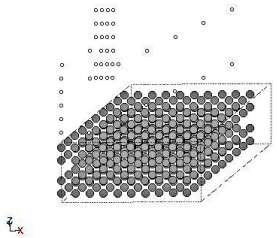

Figure 1. Initial configuration top surface of the molecular dynamics simulation model

In the study the reliability function of the two-parameter Weibull distribution to assess the material's reliability. This information is used by the 2-parameter Weibull distribution's reliability function to evaluate the material's dependability. A major objective of the literature is to investigate the fusion plasma material interactions in the wall constructions of Tokamak fusion reactors. In temperature-changing chambers, plasma-material interactions take place similarly to how tritium plasma modifies the surface of the reactor inner chamber materials. For example, lifecycle reliability estimates and design are needed for graphene on the walls of the Tokamak nuclear fusion reactor when tritium retentions are present. The only studies in the literature that address tritium plasma retention, tritium redepositing, and the boronization effects of the tritium in fusion reactor studies are Tritium Retention Breeding and Tritium Retention in the Gaps of Tungsten Wall Structures of the JET, MAST, EAST, and ITER DEMO experimental fusion reactors. Being the first structural reliability investigation on the retention of tritium on the material structures of graphene reactor walls, this work closes a gap in the literature.

2. Materials and Methods

2.1. Materials

Molecular dynamics simulations were conducted utilizing the Python programming language. Version 6.0.3 of Spyder, part of the Anaconda module, was utilized to complete this task. Calculations were performed on a Dell Precision 7680 equipped with an Intel Core i7 13th Generation processor, operating on Ubuntu 24.10 Linux. The version of the Python compiler utilized was 3.12.7. This study utilizes the Atomic Simulation Environment (ASE [20]), a Python framework designed for molecular dynamics simulations in figure 2:

Figure 2. Atomic Simulation Environment in Python language for Molecular Dynamics Simulation

2.2. Methods

The retention mechanism was developed through the simulation of a significant amount of graphite, comprising approximately 1,200 carbon atoms. The findings demonstrated that retention efficacy was influenced by multiple factors, such as the pressure and temperature conditions present during the simulation. The findings have important implications for future research on carbon-based materials and their diverse applications across various sectors. Graphene is treated as the C hexagonal crystal structure. For the sake of simplicity size of the simulated material molecular calculations tritium is treated with the single hydrogen atoms. In the molecular dynamics Carbon atoms in Figure 2 symbolized in gray color and the tritium (hydrogen) atoms in Figure 2 are given as white color. The block underwent exposure to hydrogen at energy levels between 5 and 35 keV with 3T magnetic induction force to enable calculations and substitute tritium. The selected energy levels for the simulation were adequate, as demonstrated by the current simulations covering a suitable range of collision energy, as reported in the literature. Initialization of the molecular dynamics algorithm parameters are stated below:

```
# Parameters
a1 = 2.46 # Lattice constant for graphene (in Angstrom)
c1 = 6.70 # Interlayer spacing for graphene (in Angstrom)
num_hydrogen_atoms = 42
timestep = 1.0 # fs
total_steps = 200
temperature = 300 # K
vacuum=True
orthogonal=True
periodic=True
bulk_cutoff = 5.0 # Distance cutoff for retention (Angstroms)
h = 3 #distance between tritium and graphen surface
energy_H = 5 to 35 # keV initial energies
magnetic_field = 3.0 # Magnetic field in Tesla
hydrogen_mass = 1.00784 * 1.66053906660e-27 * units.kg # Mass of hydrogen atom
hydrogen_charge = 1 * units.C # Charge of hydrogen ion (H+)
```

In this study, the potential for the simulation configurations of the materials are used is the Effective Medium Theory (EMT) potential defined in the ASE python framework. EMT is developed from averaging the multiple values of the constituents that directly make up the composite materials that are in electromagnetic environment. Effective permittivity of the materials as a whole is calculated in the acceptable approximations.

Thermal equilibrations were performed with residual graphene under controlled conditions at a temperature of 300K. A significant number of these were conducted. For one second, the surface layers were free to move due to the magnetic force hits applied by the microcanonical (NVE) ensemble. This made it easy for these layers to move. This is made possible by the mechanism that keeps the ensemble's energy, volume, and elements constant. The upper four layers were Langevin-thermostatized for one picosecond after the NVE cycle to disperse the heat generated by the bombardment.The integral of Newton's Second Law of Motion is employed to simulate the motion of a group of particles (atoms or molecules) in molecular dynamics, a calculation model. The i-th atom's motion is denoted as [21]:

$$m_i x_i = -\nabla U_i \tag{1}$$

in (1) m_i is the mass, x_i is the position and U_i is an interatomic potential energy function that describes the interaction between each atom and its neighbors. The molecular dynamics simulation of the hcp function of ASE generates a graphene structure within a substantial graphite crystal. The hydrogen atoms are randomly dispersed within the graphite lattice, with a starting kinetic energy ranging from 5 keV to 35 keV with an electromagnetic force of 3T. In molecular dynamics simulations, the Velocity-Verlet approach is employed to simulate the system's dynamics [22-24]. Then in the simulation kinetic energy based Shannon Entropy is computed to the system simulation model configuration. Utilizing the atom positions corresponding kinetic energies, we compute the Shannon entropy of the system in this simulation. According to Shannon, the set of probabilities can be identified as p1, p2, p3,..., pn, which results in vagueness through (H) measurement. The Shannon entropy is provided as [25-26] when the atoms' positions in this system model are implemented:

$$H = K \sum_{i=1}^{n} p_i log_2 p_i \tag{2}$$

The Shannon entropy and associated probabilities p1, p2, p3,..., pn are displayed in Equation (2). These probabilities relate to the atomic model used to set up the system in molecular dynamics and the frequency of atom appearance. The calculation of the Shannon

Entropy is performed by using the kinetic energy values of the corresponding atom positions. Each kinetic energy information is selected with the bins of 50 and based on the sampled bins the histogram is calculated. Based on the histogram and the summation of the histogram probabillity is derived and by using (2) formulation Shannon Entropy based on the kinetic energy values are calculated. The Weibull reliability distribution is defined by the calculated kinetic energy based Shannon entropy values. Based on the above procedure, Kinetic Energy based Shannon Entropy is then used to calculate the material reliability calculation based on Weibull distribution. The three-parameter Weibull distribution equation is as follows [27-28].

$$R(t) = e^{-(\frac{t-\gamma}{\alpha})^{\beta}} \quad (3)$$

where t denotes the irradiation duration (), γ is the location parameter, β is the shape parameter (slope) (β>0), and α is the scale parameter (characteristic life) (α>0). In computations, it is a widely held belief that γ=0, as it denotes the displacement of the origin in the dependability distribution graph. The probability-of-failure function is defined as follows:

$$F(t) = 1 - R(t) \quad (4)$$

$$1 - F(t) = e^{-(\frac{t}{\alpha})^{\beta}} \quad (5)$$

In the previously mentioned context, γ equals zero, and the specified conditions for F(t) are 0 < F(t) < 1. In order to satisfy the mandated criteria, the equation is adjusted.

$$ln(ln\frac{1}{1-F(t)}) = \beta lnt - \beta ln\alpha \quad (6)$$

The following is generated when the equation is created in the configuration of y=mx+n:

$$y(t) = ln(ln\frac{1}{1-F(t)}), \; m=\beta \text{ and } n=-\beta ln\alpha \quad (7)$$

Bernard Approximation for Median Ranks is utilized to calculate the unreliability parameters for each failure [31]. Then the unreliability parameter became:

$$F(t) = MedianRank = \frac{Rank-0,3}{N+0,4} \quad (8)$$

where N is the dataset's maximum number of orders, and rank is the order number in the tables given in the results section.

3. Results and Discussion

The simulation bombards the graphene crystal with hydrogen ions at energies ranging from 5 keV to 35 keV, utilizing a magnetic field strength of 3T. The next phase of the procedure entails the execution of molecular dynamics simulations. Graphene construction comprises multiple layers to facilitate the integration of thermostats. This sequence demonstrates the Shannon Entropy based on the kinetic energy calculations of the molecular configuration, as well as the three-dimensional molecular dynamics simulation results. The duration of the simulation process, the retention count from the molecular simulation model, the rank, the F(t) function, the natural logarithm of the kinetic energy based Shannon Entropy, the y(t) function linked to the kinetic energy Shannon Entropy, and the reliability based on the y(t) function for tritium affected by kinetic energies between 5 keV and 35 keV with a 3T magnetic induction force are all shown in Tables 1, 2, 3, and 4.

Table 1. Kinetic energy based Shannon Entropy F(t) and y(t) values calculated by equations 3, 4, 5, 6 and 7 for Tritium with 5keV bombardment with 3T on Graphene Crystal

Process Time (fs)	Kinetic Energy Shannon Entropy of the total bulk surface	Rank	F(t)	Ln (Shannon Kinetic Eng)	y(t)_ Shannon Kinetic Eng
0	-4	1	0,074468085	0	1
25	4	2	0,180851064	1,386294361	0,206529857
50	5,8	3	0,287234043	1,757857918	0,176563403
75	6	4	0,393617021	1,791759469	0,159948474
100	5,75	5	0,5	1,749199855	0,148611365
125	5,65	6	0,606382979	1,731655545	0,140090081
150	5,7	7	0,712765957	1,740466175	0,133310901
175	5,9	8	0,819148936	1,774952351	0,127711149
200	5,95	9	0,925531915	1,78339122	0,122960135

Table 2. Kinetic energy based Shannon Entropy F(t) and y(t) values calculated by equations 3, 4, 5, 6 and 7 for Tritium with 15keV bombardment with 3T on Graphene Crystal

Process Time (fs)	Kinetic Energy Shannon Entropy of the total bulk surface	Rank	F(t)	Ln (Shannon Kinetic Eng)	y(t)_ Shannon Kinetic Eng
0	-4	1	0,074468085	0	1
25	4,95	2	0,180851064	1,599387577	0,198968365
50	5,8	3	0,287234043	1,757857918	0,168116675
75	5,98	4	0,393617021	1,788420568	0,151118198
100	6,1	5	0,5	1,808288771	0,139573118
125	6,3	6	0,606382979	1,840549633	0,130928245
150	6,5	7	0,712765957	1,871802177	0,124072886
175	6,45	8	0,819148936	1,864080131	0,118426234
200	6,55	9	0,925531915	1,87946505	0,11364758

The latest column in the table 1,2,3,4 determines the reliability values based on kinetic energy based Shannon Entropy. For the latest column the reliability characteristic graphs for the system is drawn for comparing it to the Weibull hazard probability distribution graph. Figures 3, 4, 5, and 6 present the kinetic energy-based Shannon entropy and the corresponding graphs, respectively:

Upon observing Figures 3, 4, 5, and 6, both graphs exhibit a resemblance to the Weibull distribution probability density function associated with the hazard function. In which the R2 values of graphical fit test results are calculated and the graphical fit given for the Weibull probability fit test plots are given in the following figures 7, 8, 9, and 10.

Table 3. Kinetic energy based Shannon Entropy F(t) and y(t) values calculated by equations 3, 4, 5, 6 and 7 for Tritium with 25keV bombardment with 3T on Graphene Crystal

Process Time (fs)	Kinetic Energy Shannon Entropy of the total bulk surface	Rank	F(t)	Ln (Shannon Kinetic Eng)	y(t)_ Shannon Kinetic Eng
0	-4	1	0,074468085	0	1
25	3,75	2	0,180851064	1,32175584	0,18345641
50	5	3	0,287234043	1,609437912	0,150723429
75	5,85	4	0,393617021	1,766441661	0,132965227
100	5,9	5	0,5	1,774952351	0,121042209
125	5,95	6	0,606382979	1,78339122	0,112197999
150	5,85	7	0,712765957	1,766441661	0,105240905
175	6,2	8	0,819148936	1,824549292	0,099551042
200	6,25	9	0,925531915	1,832581464	0,094766473

Table 4. Kinetic energy based Shannon Entropy F(t) and y(t) values calculated by equations 3, 4, 5, 6 and 7 for Tritium with 35keV bombardment with 3T on Graphene Crystal

Process Time (fs)	Kinetic Energy Shannon Entropy of the total bulk surface	Rank	F(t)	Ln (Shannon Kinetic Eng)	y(t)_ Shannon Kinetic Eng
0	-4	1	0,074468085	0	1
25	3,85	2	0,180851064	1,348073148	0,205324751
50	5,75	3	0,287234043	1,749199855	0,175198344
75	6	4	0,393617021	1,791759469	0,158511436
100	5,95	5	0,5	1,78339122	0,147133639
125	5,9	6	0,606382979	1,774952351	0,138586928
150	5,8	7	0,712765957	1,757857918	0,131791019
175	5,75	8	0,819148936	1,749199855	0,126179989
200	5,85	9	0,925531915	1,766441661	0,121421338

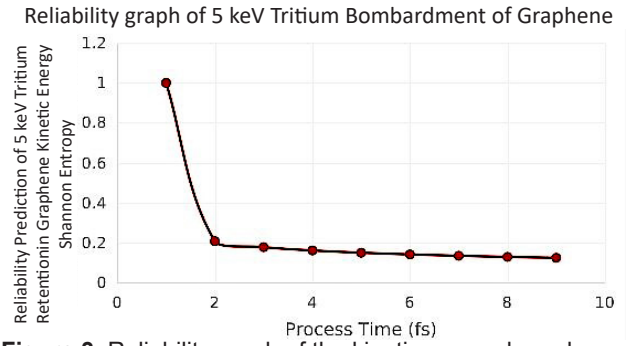

Figure 3. Reliability graph of the kinetic energy based Shannon Entropy of the simulated system at 5keV bombardment of Tritium with 3T magnetic induction force

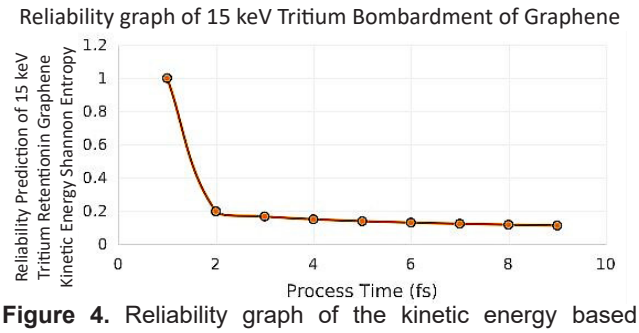

Figure 4. Reliability graph of the kinetic energy based Shannon Entropy of the simulated system at 15keV bombardment of Tritium with 3T magnetic induction force

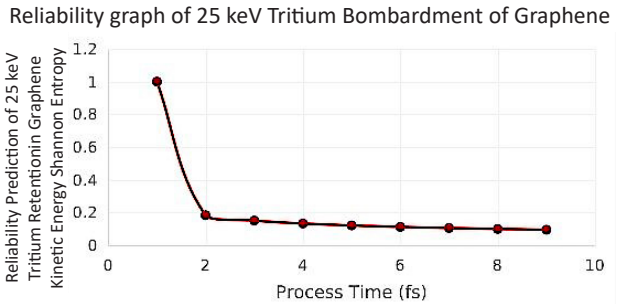

Figure 5. Reliability graph of the kinetic energy based Shannon Entropy of the simulated system at 25keV bombardment of Tritium with 3T magnetic induction force

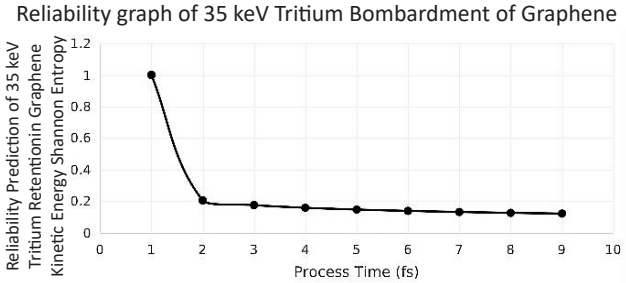

Figure 6. Reliability graph of the kinetic energy based Shannon Entropy of the simulated system at 35keV bombardment of Tritium with 3T magnetic induction force

The Figure 7 shows the transformed data points against the theoretical quantiles of Weibull distribution for 5 keV tritium plasma process of Shannon Entropy calculated based on kienitc energy. The points roughly follow the red regression line, with the R2=0.8718 which shows that the Weibull distribution is a good fit for Shannon Entropy based on kinetic energy at 5 keV energy of tritium plasma.

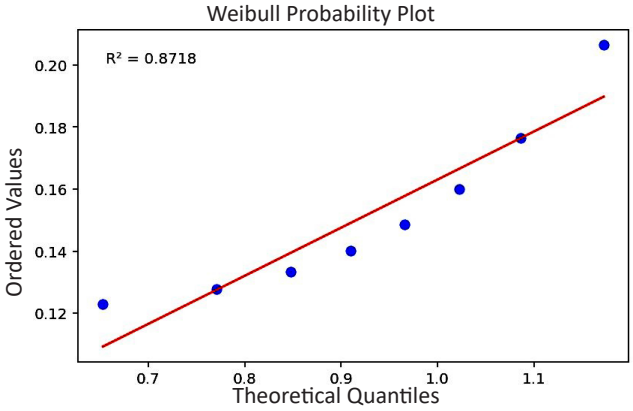

Figure 7. Graphical Fit Test Weibull Probability Plot for 5keV based tritium Shannon Entropy calculated based on kinetic energy

The Figure 8 shows the transformed data points against the theoretical quantiles of Weibull distribution for 15 keV tritium plasma process of Shannon Entropy calculated based on kienitc energy. The points roughly follow the red regression line, with the R2=0.8395 which shows that the Weibull distribution is a good fit for Shannon Entropy based on kinetic energy at 15 keV energy of tritium plasma.

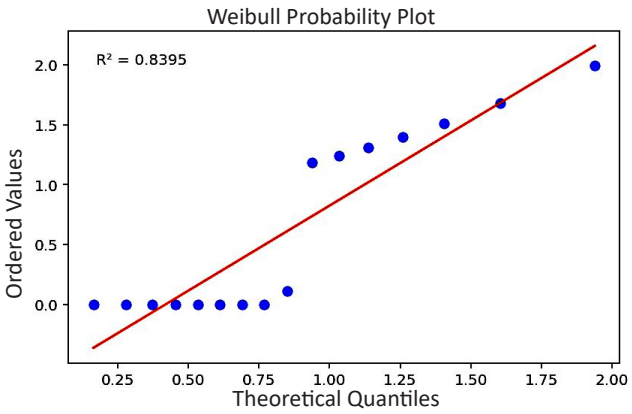

Figure 8. Graphical Fit Test Weibull Probability Plot for 15keV based tritium Shannon Entropy calculated based on kinetic energy

The Figure 9 shows the transformed data points against the theoretical quantiles of Weibull distribution for 25 keV tritium plasma process of Shannon Entropy calculated based on kienitc energy. The points roughly follow the red regression line, with the R2=0.8105 which shows that the Weibull distribution is a good fit for Shannon Entropy based on kinetic energy at 25 keV energy of tritium plasma.

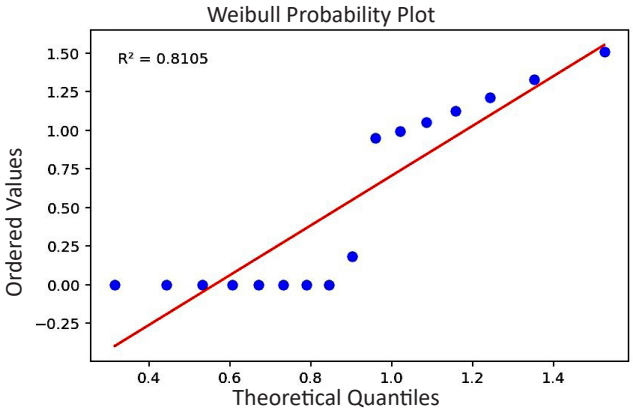

Figure 9. Graphical Fit Test Weibull Probability Plot for 25keV based tritium Shannon Entropy calculated based on kinetic energy

The Figure 10 shows the transformed data points against the theoretical quantiles of Weibull distribution for 35 keV tritium plasma process of Shannon Entropy calculated based on kienitc energy. The points roughly follow the red regression line, with the R2=0.7797 which shows that the Weibull distribution is a good fit for Shannon Entropy based on kinetic energy at 35 keV energy of tritium plasma. As the applied kinetic energy of tritium plasma is increased from 5keV to 35keV the calculated Shannon Entropy based on the molecular dynamics system calculated kinetic energy the Entropy of irregularities are increased. For instance all of the calculated 5keV, 15keV, 25keV and 35keV corresponding Shannon Entropies based on system kinetic energy calculated Weibull distribution reflect the same approximate values. It is obvious the system is unreliable and show the effect of the retention because of the tritium atoms are bounded to the graphene “C” atoms to hold them in the crystal structure.

4. Conclusions

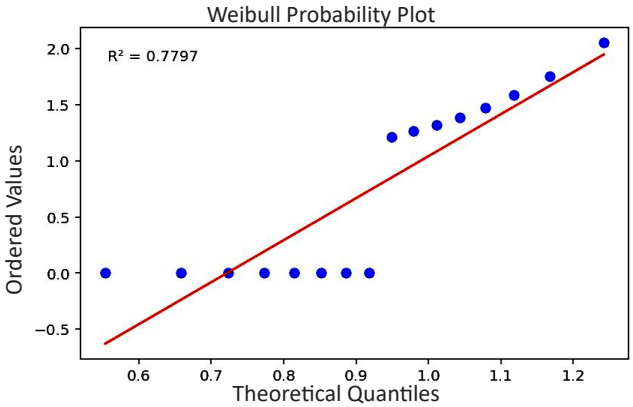

Figure 10. Graphical Fit Test Weibull Probability Plot for 35keV based tritium Shannon Entropy calculated based on kinetic energy

The material choices required for plasma-based energy devices, such as fusion Tokamak reactors and space propulsion systems, are assessed by the graphs presented in the previous results. The estimated results indicate that the Weibull distribution, which incorporates Shannon entropy calculations based on the system kinetic energy, is a valuable method for evaluating the reliability of structures when they interact with plasma and materials. From the given results above the Shannon Entropy based on the kinetic energy of the system can be used as a feature in determining the reliability prediction of the structure materials. Since this study is based on molecular dynamics simulations for tritium plasma interaction with the graphene, the experimental tokamak reactor fusion with graphene wall materials during the operational effects of tritium plasma as a fuel in fusion process is necessary to perform for future studies. In the computation of the structural reliability of events that entail contact with plasma material, the Weibull distribution is advantageous. This study complemented the objective of Shannon Entropy based on the system kinetic energy parameter based Weibull distribution prediction can be used in the reliability calculation of the fusion reactor wall structures. So that the nuclear fusion reactor wall material selection and design criteria can use the Weibull reliabilities calculated parameters as a requirement by the designers of the tokamak type fusion reactors. Likewise the nuclear fission sector use the structural reliability in pumps and pipes, nuclear fusion Tokamak type of reactors will utilize this technique with the same perspective in the structural components of vacuum vessel, In-vessel, test blanket modules and diagnostics. The Weibull method can be employed to examine plasma material interactions in forthcoming studies of plasma parameters. Future

investigations on plasma collisionality and anode/cathode sputtering are viable. The operational efficacy, safety, and security of Tokamak fusion reactors are ensured by their structural integrity. This includes the selection of appropriate materials, the assessment of wear and damage via surface roughness measurements, the management of heat and stress during plasma operations, the application of Weibull analysis to gauge reliability, and the implementation of regular maintenance.

Author Contribution Statement

The study's conception and design were the collaborative efforts of all authors. The authors themselves conducted the material preparation, data collection, and analysis.

References

[1] Ongena J., "Nuclear fusion and its large potential for the future world energy supply", 2016, Nukleonika Journal, pp:425-432, web site ref: https://sciendo.com/pdf/10.1515/nuka-2016-0070

[2] Takeda S., Pearson R.Nuclear Fusion Power Plants. Power Plants in the Industry. 2018; Chap 6: 101-122, IntechOpen publishing, website ref: https://www.intechopen.com/chapters/62970, DOI: 10.5772/intechopen.80241

[3] IAEA.Fusion Energy for Peace and Sustainable Development. IAEA. Vienna. 2018: 2-18. web site ref: https://nucleus.iaea.org/sites/fusionportal/SiteAssets/18-03925E_BRO_Fusion.pdf

[4] IAEA.Kikuchi M., Lackner K., Tran M. Q.Fusion Physics. Vienna. 2012: 20-21, web site ref: https://wwwpub.iaea.org/MTCD/Publications/PDF/Pub1562_web.pdf

[5] Ibrahim S., Lahboub F. Z., Brault P., Petit A., Caillard A., Millon E., Sauvage T., Fernandez A., Thomann A.L.Influence of helium incorporation on growth process and properties of aluminum thin films deposited by DC Magnetron sputtering.Surface and Coatings Technology.2021; Vol;426, web site ref: https://www.sciencedirect.com/science/article/abs/pii/S0257897221009828, https://doi.org/10.1016/j.surfcoat.2021.127808

[6] Behrish R., Harries D. R.International Atomic Energy Agency.Lifetime Predictions For The First Wall and Blanket Structure of Fusion Reactors.Proceedings of a Technical Committee Meeting.Karlsruhe. Nuclear Fusion J. 1986; Vol: 26, DOI 10.1088/0029-5515/26/5/015

[7] IoP Publishing Ltd. Nuclear Fusion Half a Century of Magnetic Confinement Fusion Research.2002:230-258, web site ref: https://library.psfc.mit.edu/catalog/online_pubs/conference%20proceedings/fusion%20energy%20conferences/Nuclear%20Fusion%20(IOP)%20half%20a%20century.pdf

[8] Kotov V.Particle conservation in numerical models of the tokamak plasma edge. Physics Plasma Ph Archive. Forschungszentrum Jülich GmbH, Institut für Energie- und Klimaforschung-Plasmaphysic.Partner of the Trilateral Euregio Cluster.Jülich, Germany, 2017; Vol 24, https://doi.org/10.1063/1.4980858

[9] K. Wojcyzkowski. New Development in Corrosion Testing: Theory, Methods and Standards.AESF Foundation, Plating and Surface Finishing.2011; Vol January, web site ref: https://www.pfonline.com/articles/new-developments-in-corrosion-testing-theory-methods-andstandards

[10] Linden T.Compact Fusion Reactors.CERN Colloquium. Helsinki Institute of Physics 2015; Vol March, web site ref: http://cds.cern.ch/record/2004827

[11] L. Rajablou, S.M. Motevalli, F. Fadaei.Study of alpha particle concentration effects as the ash of deuterium-tritium fusion reaction on ignition criteria.Physica Scripta.2022; Vol 97, No 9: DOI 10.1088/1402-4896/ac831a

[12] Malo M., Morono A., Hodgson E. R.Plasma Etching to Enhance the Surface Insulating Stability of Aluminumina for Fusion Applications.Nuclear Materials and Energy. Elsevier.2016; Vol 9: 247-250, DOI:10.1016/j.nme.2016.05.008

[13] Miyamoto K.Fundamentals of Plasma Physics and Controlled Fusion.2011.3rd Edition: 1-21, web site ref: https://www.nifs.ac.jp/report/NIFS-PROC-88.pdf, DOI 10.1088/0029-5515/38/4/701

[14] Cronvall O., "Structural lifetime, reliability and risk analysis approaches for power plant components and systems", Espoo 2011, pp. 69, VTT Publications 775.

[15] Arena P., Maio P. A.Special Issue .Structural and Thermo-Mechanical Analysis in Nuclear Fusion Reactors.MDPI Applied Sciences.2020;web site ref: https://www.mdpi.com/journal/applsci/special_issues/Fusion_Reactors, https://doi.org/10.3390/app122412562

[16] Apostolakis G. E., Sanzo D. L. Limiter Probabilistic Lifetime Analysis. Fusion Engineering and Design. 1988;Vol. 6:229-267, https://doi.org/10.1016/S0920-3796(88)80111-X

[17] Du, X.Unified Uncertainty Analysis by the First Order Reliability Method.J. Mech. Des. 2008; Vol 30 (9): 091401-09410, DOI:10.1115/1.2943295

[18] Freidberg J.P., Mangiarotti F.J., Minervini J. Desgining a Tokamak Fusion Reactor-How Does Plasma Physics Fit In?. Plasma Science and Fusion Center.Massachusetts Insitute of Technology, Cambridge MA.2015; Vol June; 16.,https://doi.org/10.1063/1.4923266

[19] Fusion Energy Sciences Workshop.On Plasma Material Interactions-Report on Science Challanges and Research Opportunities in Plasma Material Interactions. U.S. Department of Energy, Office of Science, France, Fusion Energy Sciences, 2015

[20] Ask Hjorth Larsen, Jens Jørgen Mortensen, Jakob Blomqvist, Ivano E. Castelli, Rune Christensen, Marcin Dułak, Jesper Friis, Michael N. Groves, Bjørk Hammer, Cory Hargus, Eric D. Hermes, Paul C. Jennings, Peter Bjerre Jensen, James Kermode, John R. Kitchin, Esben Leonhard Kolsbjerg, Joseph Kubal, Kristen Kaasbjerg, Steen Lysgaard, Jón Bergmann Maronsson, Tristan Maxson, Thomas Olsen, Lars Pastewka, Andrew Peterson, Carsten Rostgaard, Jakob Schiøtz, Ole Schütt, Mikkel Strange, Kristian S. Thygesen, Tejs

Vegge, Lasse Vilhelmsen, Michael Walter, Zhenhua Zeng, Karsten Wedel Jacobsen, “The Atomic Simulation Environment—A Python library for working with atoms”, Phys.: Condens. Matter Vol. 29 273002, 2017

[21] Gonzalez A. M., “Force Fields and Molecular Dynamics Simulations”, pp: 169-200, EDP Sciences, 2011

[22] Bedoya F., “Plasma facing components conditioning techniques and their correlation with plasma performance in the national spherical Torus experiment upgrade (NSTX-U)”, [Doctoral Dissertation]. Urbana-Champaign, IL: University of Illinois at Urbana-Champaign, Illinois Digital Environment for Access to Learning and Scholarship 2017. Available at: http://hdl.handle.net/2142/99444

[23] Schneider T, Stoll E., “Molecular-dynamics study of a three-dimensional one-component model for distortive phase transitions.”, Phys Rev B (1978) 17:1302–22.

[24] Timonova M, Thijsse BJ., “Molecular Dynamics simulations of the formation and crystallization of amorphous Si”, Comput Mater Sci, 50(8):2380–90, 2011.

[25] K. Wojcyzkowski.New Development in Corrosion Testing: Theory, Methods and Standards.AESF Foundation, Plating and Surface Finishing.2011; Vol January, web site ref: https://www.pfonline.com/articles/new-developments-in-corrosion-testing-theory-methods-andstandards

[26] Karaca Y, Moonis M., “Multi-Chaos, Fractal and Multi-Fractional Artificial Intelligence of Different Complex Systems”, Chapter 14, pp:231-245, Academic Press, 2022

[27] Kotov V.Particle conservation in numerical models of the tokamak plasma edge. Physics Plasma Ph Archive. Forschungszentrum Jülich GmbH, Institut für Energie- und Klimaforschung-Plasmaphysic.Partner of the Trilateral Euregio Cluster.Jülich, Germany, 2017; Vol 24, https://doi.org/10.1063/1.4980858

[28] Asadi S. Panahi H., Anwar S., Lone S. A.Reiability Estimation of Burr Type III Distribution under Improved Adavtive Progressive Censoring with Application to Surface Coating.Eksploatacja i Niezawodnosc-Maintenance and Reliability.2023;Vol 25, Issue 2, https://doi.org/10.17531/ein/163054

TURKISH ENERGY, NUCLEAR AND MINERAL RESEARCH AGENCY
TURKISH JOURNAL OF NUCLEAR SCIENCES
E-ISSN: 2791-7185
https://dergipark.org.tr/tr/pub/tjns

Fraser Photinia shoot explantation *in vitro*: Effects of two distinct gamma-ray sources and identification of the optimal mutation dose

Onur Sinan Türkmen[1,4,*], K. Yaprak Kantoğlu[2], Ş. Şebnem Ellialtıoğlu[3]

[1] Çanakkale Onsekiz Mart University Agriculture Faculty Department of Field Crops, Çanakkale, Türkiye
[2] Turkish Energy, Nuclear and Mineral Research Agency (TENMAK), NÜKEN, Ankara, Türkiye
[3] Doqutech Academy Llc. Co., Ankara University Technopolis, Ankara, Türkiye
[4] Margeht Biotechnology Llc. Co. Canakkale Technopark, Çanakkale, Türkiye

ARTICLE INFO

Article history:
Received June 5, 2025
Available June 26, 2025

Research Article

Keywords:
EMD_{50}
in vitro mutation
Photinia fraseri
Red Robin

ABSTRACT

Because of its beautiful qualities and ability to withstand harsh conditions, Fraser photinia (*Photinia* × *fraseri* cv. Red Robin) is frequently used as an ornamental plant in garden designs. The efforts to create new, highly marketable variations of the species have begun to increase in response to the growing ability of the current kinds to adapt to changing climatic circumstances. For this species, which is susceptible to *in vitro* propagation, the *in vitro* mutation breeding technique holds significant promise for increasing the current variety. It is essential to ascertain whether ionizing gamma ray sources are suitable for in vitro mutation investigations on Fraser photinia. To achieve this, *in vitro* shoot explants were exposed to a total of thirteen different radiation doses using ^{60}Co (dosage rate: 235 Gy/h) and ^{137}Cs (dosage rate: 821 Gy/h) gamma ray sources. The number of leaves and shoot length in *in vitro* plantlets were assessed thirty days after irradiation, and linear regression analysis was used to get the effective mutation dose (EMD_{50}) values. Based on the quantity of leaves, the EMD_{50} for the ^{137}Cs source ray application was 60.34 Gy, whereas the ^{60}Co source resulted in an EMD_{50} of 80.88 Gy. These findings demonstrated that the EMD_{50} difference was significantly impacted by the source power, irradiation duration, and the influence produced by the linear energy transfer value of the irradiation during tissue penetration.

1. Introduction

Plants are essential to landscape design for both functional and aesthetic reasons. The use of materials, particularly plant elements, has improved and diversified, and each section of the landscape design has been converted into areas that require specialization [1]. Because of the effects of climate change, the use of plant species that are not commonly found in the natural flora and are therefore not naturally grown in a region raises the value of landscaping [2, 3]. However, the plants chosen for landscaping should also be able to adapt to the local climate.

The evergreen, attractive woody shrub *Photinia* × *fraseri* Dress. (Fraser photinia, Fraser's photinia) is commonly planted in green spaces and can reach a height of three to five meters. This species, which is a member of the *Rosaceae* family, is a hybrid of Chinese *Photinia serrulate* and Japanese *Photinia glabra. Photinia* × *fraseri* is a popular hedge and decorative plant for parks, gardens, and roadside landscaping because of its striking leaf traits, colors, and quick growth. The leaves of this plant are either red (young leaves) or green (mature leaves). Because the young, bright red leaves contrast with the older, dark green ones, the perennial foliage is particularly stunning when it first sprouts [4]. Its perennial foliage is striking throughout the sprouting process because of its vivid crimson-red color, and its oblong, flat, glossy leaves are tolerant to cold. Large white terminal clusters are produced throughout the spring flowering season [5]. In addition to being aesthetically beautiful, this hedging plant gives the garden texture and acts as a useful windbreak. Additionally, Photinia plants' vibrant red leaves and open growth attract birds and other wildlife, fostering a happy coexistence of nature and the garden [6].

Photinia × *fraseri* 'Red Robin' is the most popular cultivar [7]. The hybrid plant originated from Fraser Nursery in Alabama (hence its name), but the 'Red Robin' was later developed in New Zealand [8]. A notable characteristic of photinia 'Red Robin' is its eye-catching leaves.

The evergreen shrub Photinia 'Red Robin', on the other hand, not only endures but flourishes in harsh environments. Because of its remarkable cold tolerance, Photinia 'Red Robin' is a great choice for areas with severe winters. The Red Robin cultivar, whose cold tolerance level is stated to be between -17.7 to -15.0 °C, can also be evaluated in different climatic conditions in urban planning as a plant with high temperature (+43.6 to +46.3 °C) [9]. Once

*Corresponding author: onurturkmen@comu.edu.tr

established, it can endure dry spells without losing its aesthetic appeal. It can obtain moisture from deeper in the earth because of its extensive root system, which guarantees its survival during dry spells. Strong winds can make it difficult for plants to stay healthy and in shape. However, Photinia 'Red Robin' has exceptional wind resistance. It withstands wind effectively thanks to its strong branches and resilient leaves. As long as the soil drains properly, it can grow in a variety of soil types, including clayey, sandy, and loamy soils [10]. Improvement of clay soils with organic matter to allow roots to breathe and develop can be done by using organic matter such as biochar and barnyard manure or inorganic matter such as sand that lightens the soil structure. Although Red Robin photinia is quite tolerant to adverse environmental conditions, it is particularly sensitive to alkaline soils with high pH [7, 11] or high salinity conditions [12, 13].

While intensive research focuses on field crops and vegetables; breeding programs for ornamental plants, especially perennial plants, remain limited. The basis of plant breeding is the presence of genetic variation in the plant material under study. This variation can be obtained by selection, hybridization, and techniques from natural populations. According to the study by Özel et al. [14], “ortet selection” can boost Fraser photinia seedling performance many times. This study shows that genetic variation exists in the photinia species. The producers' profit rate will rise significantly if the fastest-growing ortets are chosen for the seedlings grown for landscaping since they will be able to reach a marketable size more quickly.

Studies mainly carried out in the last 50 years have shown that, especially in self-pollinating plants, genetic mutations confer significantly higher benefits in the development of traits than those governed by single genes and showing simple inheritance as reported by Anonymous [15], Waycott et al. [16], and Sağel et al. [17]. Abiotic stress tolerance, early, everlasting, and abundant flowering, altered photoperiodic response, and enhanced disease resistance are among the physiological properties that have been successfully mutated. Conventional breeding has contributed greatly to improving brush traits, but mutation breeding may provide an important complementary technique for improving stress tolerance and productivity. When combined with *in vitro* procedures, mutation induction and desired trait selection provide several benefits over traditional approaches [18].

Schum [19] reported that the use of gamma radiation in the use of physical mutagens is easy to use, highly permanent, accessible to target cells, and has an absence of toxic effects and damage. According to Maliga [20] and Ahloowalia [21], *in vitro* methods allow cells to be uniformly treated with physical and chemical mutagens and grown in homogeneous medium. *In vitro* cultures offer significant advantages for identifying somaclonal variation in plant breeding studies. *In vitro* mutagenesis experiments can be performed on large populations, in limited space, and at any time of the year. The chances of obtaining potent mutants are higher with *in vitro* mutagenesis. The main advantage of this method is that it avoids the formation of chimeras in M1V1. Large populations can be managed using tissue culture for mutagenesis treatment, selection, and cloning of specific mutants. It also enables quick subculture propagation cycles that separate mutated from non-mutated sectors [22]. Kane et al. [23], discussed the importance of mutation to produce phenotypic differences in Fraser photinia. They worked to develop an optimal propagation protocol in tissue culture to obtain a large number of plants for *in vitro* propagation of mutant plant material and selection.

When the studies on mutation breeding are evaluated in general, it is seen that ionizing radiation sources (such as gamma, X-ray, fast neutron, electron accelerator, and heavy ion sources) are used more heavily than chemical mutagens due to their ease of application [24]. Each ionizing radiation source is categorized by the Linear Energy Transfer (LET) value they have according to its ionization capacity [25]. Accordingly, ^{60}Co and ^{137}Cs, which are gamma ray sources, are sources with low LET levels [26, 27].

In the first phase of our studies to obtain new mutant lines tolerant to high salinity and pH levels from Red Robin photinia, it was planned to create new variations in *in vitro* shoot culture using the gamma irradiation technique. If we compare gamma radiation sources in terms of safety in the event of a nuclear or possible radiological accident, ^{60}Co sources have a lower risk of radiation pollution, contamination, and nuclear pollution compared to ^{137}Cs. When the two sources are compared in terms of energy, the energy, aggressiveness, and dose rate of ^{60}Co sources are higher than ^{137}Cs. Before starting the mutation breeding study with either gamma sources or other ionizing radiation sources, it is necessary to determine the EMD_{50} specific to the genotype to be studied as a preliminary study for the creation of the main mutant population [28, 29].

In the study whose results are presented here, it was aimed to compare the effects of the source effect as a result of irradiating the *in vitro* shoots of the Fraser’s photinia cv. Red Robin with two different gamma ray sources, ^{60}Co and ^{137}Cs, which have different dose rates and energies, and to determine the EMD_{50} according to both sources.

2. Materials and Methods

2.1. Material

In vitro Red Robin photinia shoots obtained from a commercial nursery company producing Fraser photinia via tissue culture were used as material in the research.

2.2. Methods

2.2.1. Plant culture conditions and multiplication of shoots

In this study, explants taken from stock cultures available in our laboratory were used. Therefore, no pre-sterilization process was performed on the explants. Main and lateral shoots were cut into nodal segments of similar size (7-8 mm). First proliferation media prepeared according to Larraburu et al. [30], the basic culture medium (BM) included 0.7% agar, 100 mgl^{-1} myoinositol, B5 vitamins [31], 3% sucrose, and Murashige and Skoog (MS) salts [32]. After bringing the pH down to 5.8, it was autoclaved for 20 minutes at 121°C. Explants transferred to 660 ml flasks with 50 ml of medium, supplemented with 2.2 µM BA and 0.5 µM IBA concentration. The cultures were incubated under LED illumination (55 µmol m−2 s−1) with a 16-hour photoperiod at 24 ± 2 °C and 55-60% relative humidity in a growth chamber. Shoot pieces of approximately 2 cm in length with a node on them were propagated in proliferation medium. Red Robin shoots that were sub-cultured 4 times, every four weeks, were transferred to MS [32] medium explained below.

2.2.2. Determination of Effective Mutation Dose

Two cm-long photinia shoots were cultured *in vitro* in the nutrient medium, and they were irradiated in eleven different doses (0, 10, 20, 30, 40, 50, 60, 70, 90, 110, and 130 Gy) with ^{60}Co (dose rate: 235 Gy/h) and ^{137}Cs (dose rate: 821 Gy/h) gamma ray sources within the Nuclear Energy Research Institute of the Turkish Energy Nuclear and Mineral Research Agency (TENMAK-NÜKEN) (Figure 1).

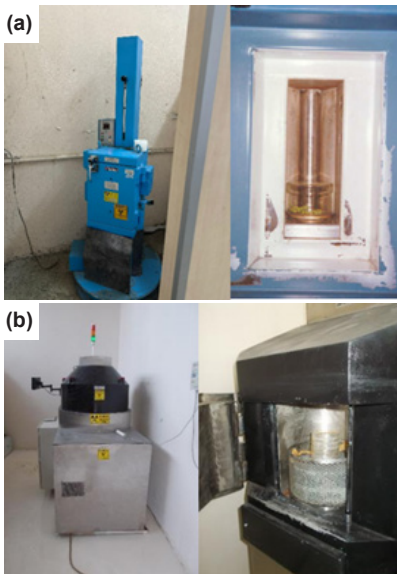

Figure 1. ^{137}Cs Research Irradiator (a); Ob-Servo Sanguis ^{60}Co Research Irradiator model (b).

As a general approach for *in vitro* explants, irradiation doses between 0 and 100 Gy are preferred [17]. However, in order to determine the dose response of the current genotype, which has not been studied before, irradiation was also performed with doses up to 130 Gy in 20 Gy increments after the 70 Gy dose. For each gamma ray and treatment dose, 30 *in vitro* shoots were used in three replication (each replication has 10 explants). The shoots were placed in sterilized nutrient hormone free MS media in autoclavable plastic bags to ensure that they fit easily into the irradiators (Fig. 2a). After irradiation, all explants were rapidly transferred to the fresh proliferation medium. This step aimed to protect the explants from the toxic effects of radicals expected to be formed during irradiation. The cultures were incubated in the controlled climatic room at 24 ± 2 °C (Fig. 2b). On the 30th day following irradiation, the shoot length and number of leaves were determined according to doses. Physical effects, including damage such as yellowing, darkening, and shoot death, caused by radiation application were also observed in explants during the period following irradiation.

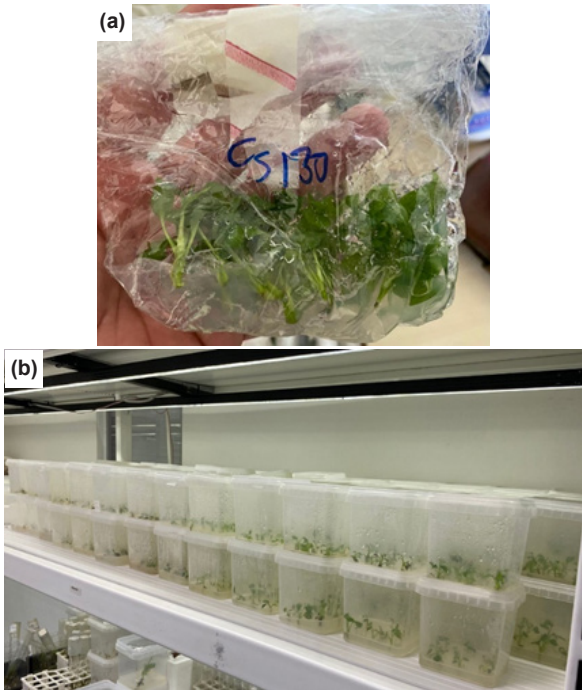

Figure 2. *In vitro* photinia shoots prepared for irradiation treatments (a); Incubation of photinia cultures after irradiation (b).

The shoot length and number of leaves data obtained after irradiation from both ionizing radiation sources were subjected to linear regression analysis to determine the EMD_{50} of the plant sample. EMD_{50} is calculated through the use of linear regression analysis by the Microsoft Excel software program [33]. In linear regression analysis, data were analyzed within a 0,95 confidence limit.

3. Results and Discussion

After irradiation at eleven different doses (control included) with ^{60}Co and ^{137}Cs gamma ray sources, all irradiated shoot tissues were sub-cultured to the fresh proliferation media to obtain shoot length evaluation and new leaves.

The study compared the shoot length and number of leaves of the test group, which received varying doses of gamma rays in both gamma ray sources, with non-irradiated non-irradiated shoots (control group). After irradiation at thirteen different doses with ^{60}Co and ^{137}Cs gamma ray sources, young leaves developed and shoot growth obtained from 30 shoots of each dose were counted 30 days after irradiation. Figure 3 shows the growth and development of irradiated photinia shoots. As a result of the observations, it was observed that the physical damage in the explants irradiated with the ^{137}Cs irradiation source was less than that of the ^{60}Co gamma source. In the ^{137}Cs source, a decreasing trend in leaf number was observed after 50 Gy application. According to Figure 4, which shows the results of the counting conducted on the 30th day following irradiation, there were notable decreases in the number of leaves as the irradiation dose increased.

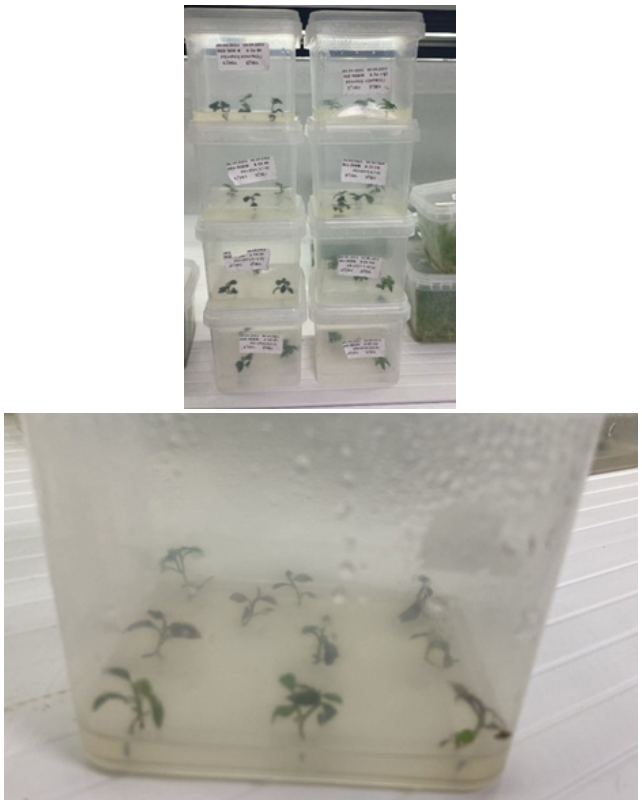

Figure 3. *in vitro* Fraser's photinia shoots developed under different irradiation treatments

This decreasing trend in shoot length was evident after a 60 Gy dose of the ^{137}Cs source. On the other hand, it was determined that the shoot length and leaf number values of the explants continued, albeit decreasingly, including the 130 Gy dose of the ^{60}Co source (Table 1). It was determined that there was a serious growth and development retardation with the 80 Gy application of the ^{60}Co source. However, it is observed in Figure 4 that the stable retardation in the cesium source could not be provided in the cobalt source. The regression analysis result performed with the data obtained as a result of irradiation with the gamma source is given in the formula (For 1.) below. In this formula, y represents

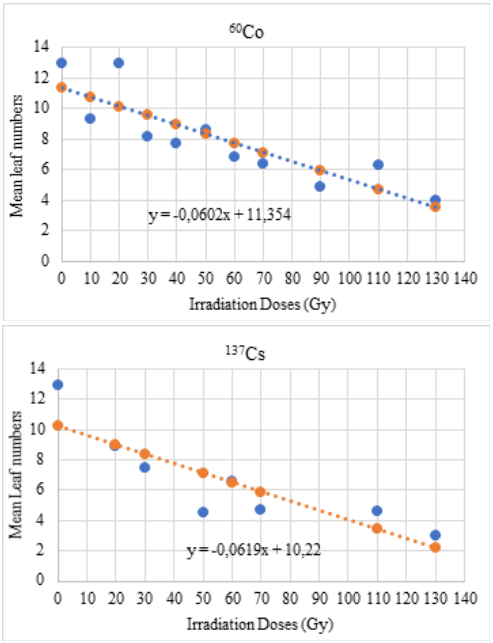

Figure 4. Graphs of leaf numbers of explants irradiated with two different gamma sources according to doses

the 50% value of the leaf number and shoot length obtained in the 0 Gy application, which is the control, while the value defined as x defines the EMD_{50}. Since the r^2 values of the average shoot values obtained after irradiation with both ionizing radiation sources were obtained below the acceptance limit of 0.74, the EMD_{50} calculation was determined based on the number of leaves that are important for this cultivar. Accordingly, the EMD_{50} was determined as 60.34 Gy as a result of ^{137}Cs (For 1). However, after being exposed to the ^{60}Co source, the EMD_{50} changed to 80.88 Gy (For 2.).

y = -0,0619x + 10,22 For 1.

y = -0,0602x + 11,354 For 2.

Today, studies on mutation breeding are carried out in many species around the world using different irradiation sources (low and high energy) [34]. Factors such as the type of biological material used

Table 1. Shoot length and leaf number of photinia explants irradiated with two different gamma sources according to doses

^{60}Co			^{137}Cs		
Dose (Gy)	**Mean shoot length (cm)**	**Mean leaf number**	**Dose (Gy)**	**Mean shoot length (cm)**	**Mean leaf number**
0	1.80	12.97	0	1.8	12.97
10	1.11	9.30	10	infected	Infected
20	1.57	13.00	20	1.24	8.87
30	1.66	8.13	30	1.29	7.43
40	1.54	7.70	40	1.01	3.43
50	1.41	8.57	50	1.56	4.53
60	1.17	6.87	60	1.48	6.57
70	1.16	6.43	70	1.32	4.67
90	1.02	4.90	90	1.05	8.60
110	1.07	6.30	110	1.21	4.63
130	1.07	4.00	130	1.05	3.00

(p value was 0,006 both cobalt and cesium sources, Sx cobalt: 1,54; Sx cesium: 1,77)

in the study (seed, *in vitro* explant, cutting, etc.) and, its water content, the LET value of the source to be irradiated, the physical and chemical effects created by the radiation source the half-life of the source used in irradiation and its dose rate and the oxygen level of the environment during application are important [26]. When the obtained findings are evaluated, the first parameter that comes to the fore is the dose rate of the source. Because the ^{137}Cs source has a higher dose rate (820 Gy/h). Although its penetration into the tissue during irradiation seems lower than the ^{60}Co source. An effective dose distribution in a short time has been provided in line with the EMD_{50} obtained for the explants. The exposed dose rate of the ^{60}Co source is 232 Gy/h, but the irradiation time is longer when compared to the ^{137}Cs source and therefore, especially for *in vitro* material the formation of free radicals in the nutrient medium is accelerated and the amount of oxygen decreases accordingly, and it is possible to create different effects on the explants [35, 36]. Similar effects and findings have been revealed in studies conducted by different researchers [26, 27, 36, 37].

Conclusions

In vitro mutation breeding studies continue to be widely used to increase the gene pool and shorten the breeding period. In this study, *in vitro* shoot explants of Red Robin photinia were used. In order to conduct mutation breeding studies with a mutant population with a wide variation, the EMD_{50} should be determined according to the genotype, explant type, and mutagen source to be used in mutation induction. As a result of the irradiation of *in vitro* shoot explants with ^{60}Co and ^{137}Cs gamma radiation, differences in absorbed doses were revealed due to source power, linear energy transfer values, and irradiation duration. Accordingly, the EMD_{50} dose limits that should be applied for the creation of an effective *in vitro* mutant population are;

- For the ^{60}Co source, the EMD_{50} is 80.88 Gy; the 10% lower and upper limits of this dose are determined as ~73 - 89 Gy.
- For the ^{137}Cs source, the EMD_{50} is 60.34 Gy; the 10% lower and upper limits of this dose are determined as ~54 - 66 Gy.

The number of leaves was found to be an appropriate parameter in determining the EMD_{50}, but the shoot length did not give the expected critical value depending on the explant type and genotype response. In this study, the EMD_{50} in two different gamma radiation sources differed. The difference between the dose rate of the sources and the irradiation time of the samples depending on this dose rate, was observed clearly in terms of leaf numbers and shoot lengths. Thus, the importance of determining the EMD_{50} using the appropriate evaluation parameter in *in vitro* mutation breeding studies and the need for dose planning accordingly were revealed. It is expected that low-energy ionized sources, such as electrically activated X-rays and electron accelerators, will replace gamma sources, especially in the next decade. It is important to start mutation breeding studies by knowing the effect mechanisms of these sources to obtain successful results.

Author Contributions Statement

Dr. Onur Sinan Türkmen: Project design, experimental work, manuscript writing.

Dr. Kadriye Yaprak Kantoğlu: Project design, irradiation, analysis of experimental work data, manuscript editing.

Prof. Dr. Şeküre Şebnem Ellialtıoğlu: Project design, manuscript editing.

Acknowledgments

This research was supported by the Margeht Biotechnology Llc. Co. The authors express their sincere gratitude to the TENMAK NÜKEN for irradiation treatment.

References

[1] Guney, K., Cetin, M., Sevik, H., Guney, K. B. (2016). Influence of germination percentage and morphological properties of some hormones practice on *Lilium martagon* L. seeds. *Oxidation Communications* 39(1): 466-474.

[2] Ayan, S., Sarsekova, D., Kenesaryuly, G., Yilmaz, E., Gülseven, O., Şahin, I. (2021). Accumulation of heavy metal pollution caused by traffic in forest trees in the park of Kerey and Janibek Khans of the city of Nur-Sultan, Kazakhstan. J*ournal of Forest Science* 67(7): 357-366. https://doi.org/10.17221/37/2021-JFS.

[3] Laaribya, S., Alaoui, A., Ayan, S., Dindaroglu, T. (2023). Changes in the potential distribution of Atlas cedar in Morocco in the twenty-first century according to the emission scenarios of RCP 4,5 and RCP 8,5. Forestist 74(3): 1-10.

[4] Bonaminio, V. P., Blazich, F. A. (1983). Response of Fraser's photinia stem cuttings to selected rooting compounds. *Journal of Environmental Horticulture* 1(1): 9-11. https://doi.org/10.24266/0738-2898-1.1.9.

[5] Brickell, C. (1996). Enciclopedia de Plantas y Flores. Royal Horticultural Society, Grijalbo Mondadori, Verona, Italy, p.566.

[6] Anonymous (2024a). Photinia Red Robin Hedge Plants. https://www.hedgingplantsdirect.co.uk/ (access date: October 2024).

[7] Anonymous (2024b). Introducing...Photinia. Common name: Christmas berry, red robin. https://www.rhs.org.uk/plants/photinia. (access date: October 2024).

[8] Anonymous (2024f). *Photinia* × *fraseri* "Red Robin." (n.d.). Missouri Botanical Garden. (https://www.missouribotanicalgarden.org/PlantFinder/PlantFinderDetails.aspx?taxonid=271346). (access date: October 2024).

[9] Anonymous (2024d). Photinia fraseri red robin wall

(ROSACEAE) Çit formlu alev çalısı. https://katalog.smsmarmaragroup.com/photinia-fraseri-red-robin-wall-rosaceae/cit-formlu-alev-calisi. (access date: October 2024).

[10] Anonymous (2024c). Thriving in the Elements: Choosing Photinia 'Red Robin' for Extreme Climates. https://duskhedges.co.nz/test-post-2/ (access date: October 2024).

[11] Anonymous (2024e). Photinia 'Red Robin' - How To Grow This Extremely Popular, Glossy-Leaved Cultivar? Horticulture Magazine, https://horticulture.co.uk/photinia-red-robin/ (access date: October 2024).

[12] Tosca, A., Valagussa, M., Martinetti, L., Frangi, P. (2021). Biochar and green compost as peat alternatives in the cultivation of photinia and olive tree. *Acta Horticulturae* 1305: 257-262 https://doi.org/10.17660/ActaHortic.2021.1305.35.

[13] Anonymous (2024g). Best Soil for Your Red Tip Photinia. https://greg.app/red-tip-photinia-soil/ (access date: October 2024).

[14] Özel, H. B., Yücedağ, C., Ayan, S. (2023). Growth performances of *Photinia* × *fraseri* Dress. seedlings from cuttings of five ortets in different districts. *SilvaWorld*, 2(2), 60-65. https://doi.org/10.61326/silvaworld.v2i2.23.

[15] Anonymous (1977). Manual on Mutation Breeding. International Atomic Energy Agency, Technical Report Series No:119. Vienna, 290p.

[16] Waycott, W., Fort, S. B. T., Ryder, E. J. (1995). Inheritance of dwarfing genes in *Lactuca sativa* L. *Journal of Heredity* 86(1): 39-44.

[17] Sağel, Z., Peşkircioğlu, H., Tutluer, I., Uslu, N., Senay, A., Taner, K. Y., Kunter, B., Sekerci, S., Yalcin, S. (2002). *Bitki Islahında Mutasyon ve Doku Kültürü Teknikleri, III: Ulusal Mutasyon Kursu Kurs Notları*, TAEK, ANTHAM Nükleer Tarım Radyobiyoloji Bölümü, Ankara (in Turkish).

[18] Çakın, I., Kunter, B., Kantoglu, K. Y., Göktuğ, A., Akyüz Çağdaş, E., Ellialtıoğlu, Ş. Ş. (2025). *In vitro* mutasyon islahı çalışmalarına yönelik olarak farklı gama ışını kaynaklarının kalanşo (Kalanchoe blossfeldiana Poelnn.) Yaprak ayası eksplantı üzerine etkilerinin karşılaştırılması. *Bahçe*, 54(Özel Sayı 1), 312-318. https://doi.org/10.53471/bahce.1539465

[19] Schum, A. (2003). Mutation Breeding in Ornamentals: An Efficient Breeding Method. Proj., 21st IS on Classical Molecular Breeding (Ed. G. Forkmann et al.), Acta. Hort. 612: 47-53.

[20] Maliga, P. (1984). Isolation and characterization of mutants in plant cell cultures. *Annual Review of Plant Physiology* 35: 519-552.

[21] Ahloowalia, B. S. (1995). *In vitro* mutagenesis for the improvement of vegetatively propagated plants. In: *Induced Mutations and Molecular Techniques for Crop Improvement*, Proceedings of IAEA/FAO Symposium. Vienna 19-23 June 1995, pp 531-541.

[22] Ahloowalia B. S., Maluszynski M. (2001). Induced Mutations- A new paradigm in plant breeding. *Euphytica* 118: 167-173.

[23] Kane, M. E., Sheehan, T. J., Philman, N. L. (1988). A micropropagation protocol using Fraser photinia for mutation induction and new cultivar selection. *Proceedings of the Florida State Horticultural Society* 100:334-337. (https://www.cabidigitallibrary.org/doi/full/10.5555/19890354891).

[24] MVD (2024). Mutant Variety database. https://nucleus.iaea.org/sites/mvd/SitePages/Search.aspx (access date: May 2024).

[25] Farkash, E. A., Kao, G. D., Horman, S. R., Prak, E. T. L. (2006). Gamma irradiation increases endonuclease-dependent L1 retrotranspositions in a cultured cell assay. *Nucleic Acids Research* 33(4): 1196-1204.

[26] Lagoda, P., Shu, Q., Foster, B., Nakagawa, H., Nakagawa, H. (2012). Effects of radiation on living cells and plant. *Plant Mutation Breeding and Biotechnology.* CABI Publishing, Wallinford, 123-124.

[27] Spencer-Lopes, M. M., Foster, B. P., Jankuloski, L. (2018). *Manual on mutation breeding third edition*. FAO Publishing, Italy, 301 pp.

[28] Turan Büyükdinç, D., Kantoğlu, K. Y., Karataş, A., İpek, A., Ellialtıoğlu, Ş. Ş. (2019). determination of effective mutagen dose for carrot (D*aucus carota ssp. sativus var. atrorubens Alef and D. carota)* callus cultures. International Journal of Scientific and Technological Research 5 (3): 15-23. https://doi.org/10.7176/JSTR/5-3-02.

[29] Kantoglu, K. Y., Sarıtoprak, O., Akyüz Çağdaş, E., Okutan, E., Aktaş, H., Ellialtıoğlu, Ş. Ş. (2024). Kalanşoda (Kalanchoe blossfeldiana Poelnn.) *in vitro* mutasyon ıslahı. *Düzce Üniversitesi Orman Fakültesi Ormancılık Dergisi,* 20(Özel Sayı), 31-43. https://doi.org/10.58816/duzceod.1537178

[30] Larraburu, E. E., Carletti, S. M., Rodríguez Cáceres, E. A., Llorente, B. E. (2007). Micropropagation of photinia employing rhizobacteria to promote root development. Plant Cell Rep. Jun;26(6):711-7. doi: 10.1007/s00299-006-0279-2. Epub 2007 Jan 5. PMID: 17205338.

[31] Gamborg, O. L., Miller, R. A., Ojima, K. (1968). Nutrient requirements of suspension cultures of soybean root cells. *Exp Cell Res* 50:151- 158. https://doi.org/10.1016/0014-4827(68)90403-5.

[32] Murashige, T., Skoog, F. (1962). A revised medium for rapid growth and bioassay with tobacco tissue cultures, *Physiol. Plant,* 15: 473- 497.

[33] Haspolat, G. (2022). Induction of mutagenesis on Chrysanthemums. *Ornamental Horticult.* 28(4): 431-441. https://doi.org/10.1590/2447-536X.v28i4.2523.

[34] Melsen, K., van de Wouw, M., Contreras, R. (2021). Mutation breeding in ornamentals. *HortScience* 56(10): 1154-1165. 2021.

[35] Micke, A., Donini, B. (1993). Induced mutations. Eds. M.D., Hayward, N., O., Bosemark, I., Romagosa. *Plant Breeding, Principles and Prospects*, Chapman & Hall, London. p52-62.

[36] Mba, C., Afza, R., Shu, Q., Shu, Q., Foster, B., Nakagowa, H. (2012). Mutagenic radiation: X-ray, ionizing particles and ultraviolet. Plant Mutation

Breeding and Biotechnology. CABI, Oxfordshire, UK. 83-90.

[37] Leonard, A., Jacquet, P., Lauwerys, R. (1983). Mutagenicity and teratogenicity of mercury compounds. *Mutation Research/Reviews in Genetic Toxicology* 11(4): 1-18.

AUTHOR'S GUIDE

GENERAL INFORMATION

• For article application, 3 individual files which are Manuscript File, Copyright Transfer File and Similarity Ratio File, must be filled in and uploaded to the system.
• Applications should include the contact information of the author and other authors to be contacted.
• The article checklist and cover page in the Manuscript File should be filled in completely.
• Each article is sent to at least two referees related to its subject and examined in terms of format, content, novelty, contribution to literature.
• If figures and tables from other publications are to be used in review articles, permission must be obtained from the publisher of the article to be cited. The information that permission has been granted from the publisher and whether the figures have been adapted or used directly should be mentioned in the figure caption. The relevant permission letter should be sent to journalofboron@tenmak.gov.tr.
• After the deficiencies stated in the referee's comments are completed, it is brought to the final print format and the approval of the final version of the article is obtained from the authors. The responsibility of errors that may be found in the article as it is published in the journal belongs to the authors.

MANUSCRIPT

• Writing rules must be followed, during writing of the manuscript.
• Inclusive and scientific language must be used in the manuscript.
• Manuscript should not exceed 14,000 words for research articles and 22,000 words for review articles, including references.
• The manuscript should be written in Times New Roman 12 points without changing the page layout of the Manuscript File.
• The manuscript should be prepared with a word processor of Microsoft Office Word 2010 and above, and spelling errors should be checked and corrected.
• Abbreviations and symbols used in the manuscript must be explained when used fort he first time.
• Subheadings in the article should be numbered. Numbering should start at 1 for the main section and continue for all main headings (except the Summary, Acknowledgments and References and Appendices sections). Secondary titles continue as 1.1., 1.2., 1.3., ... in accordance with the main chapter numbering. The third headings continue as 1.1.1., 1.1.2., 1.1.3., ... in accordance with the second headings.

COPYRIGHT TRANSFER FILE

• Signed Copyright Transfer File should be scanned and uploaded to the system.
• Applications of the authors who do not send the signed Copyright Transfer File will not be evaluated.

SIMILARITY RATIO FILE

• The manuscript should be scanned with "iThenticate" or "Turnitin" programs, except for the references section.
• The similarity ratio report should be uploaded to the system in PDF format.
• The similarity ratio should not exceed 15%.

PRIVACY POLICY

Journal of Boron respects privacy. Any personal information will only be used in line with the stated purposes of the journal and will not be shared with third parties.

WRITING RULES

TITLE
• The title of the manuscript should consist of a maximum of 15 words with standard abbreviations.

ABSTRACT
• The abstract should not exceed 250 words.
• Non-standard abbreviations should be written in parentheses after their full explanation, when they are used for the first time.

KEYWORDS
• A maximum of 5 keywords should be written in alphabetical order.
• Abbreviations should not be used as keywords.

INTRODUCTION
• The summary of the relevant literature, aim and novelty of the study, and the established hypothesis should be included.
• References should not be given in bulk and in intervals (example [1-5] or [1, 2, 3, 5, 8]), the contribution of each source to the study should be examined and stated in the text.

MATERIALS AND METHODS
• If the study carried out is an experimental study, the test procedure/method should be clearly explained.
• If a theoretical study has been carried out, the theoretical method should be given in detail.
• If the method used in the study is a previously published method, the other study should be mentioned by citing.

RESULTS AND DISCUSSION
• Obtained results should be given in a clear and concise manner.
• All of the results should be compared with the literature by citing.
• Tables should be numbered and in editable format.
• Figures in the manuscript should be numbered and have at least 300 dpi resolution. The texts on the figures should be in legible size and font. Accepted figure formats are TIFF, JPG, and JPEG.

CONCLUSIONS
• Main conclusions and inferences obtained from the study should be given concisely.
• Future perspectives of the study are given in this section.

ACKNOWLEDGEMENTS
• The financial resources provided and the infrastructure used during the study are specified in this section.

AUTHOR CONTRIBUTIONS
• Contributions of each author must be stated.
• Contribution roles are as follows: conceptualization, data analysis, data curation, funding acquisition, methodology, project administration, sourcing, software analysis, supervision, validation, visualization, writing original draft, writing review and editing.

REFERENCES
• DOI and ISBN numbers of printed sources should be specified.
• Website addresses (URLs) should not be given as a source. However, it can be specified after the data where a statistical data is mentioned in the text.
• The list of references should be numbered according to the order in which they are used in the text.
• References should be prepared in accordance with the rules of “APA Publication Manual, Seventh Edition”.
• References should be prepared in English. English equivalents of sources should be indicated in square brackets.
• APA format and examples can be found at the link below.
https://apastyle.apa.org/style-grammar-guidelines/references/examples

APPENDICES
• Appendices in the manuscript must be named as Appendix A (Appendix A), Appendix B (Appendix B) and Appendix C (Appendix C) etc.
• Equations in the appendices must be named as A1, A2, A3, etc., and table and figures numberings must be named as Table A1, Table A2, Figure A1, Figure A2 etc.

TURKISH ENERGY, NUCLEAR AND MINERAL RESEARCH AGENCY
TURKISH JOURNAL OF NUCLEAR SCIENCES
E-ISSN: 2791-7185
https://dergipark.org.tr/tr/pub/tjns

İÇİNDEKİLER/CONTENTS

TENMAK Akademik Yayınlar Koordinatörlüğü

Ankara Üniversitesi Beşevler Kampüsü, Emniyet Mahallesi, Yenimahalle 06560, Ankara, Türkiye
Tel: (0312) 212 62 30
Fax: (0312) 295 87 61
E-posta: journal@tenmak.gov.tr
Web: https://dergipark.org.tr/tr/pub/tjns